Proton, deuteron, and triton emission at target rapidity in Au+Au collisions at 10.20*A* GeV: Spectra and directed flow

L. Ahle,[8] Y. Akiba,[5] K. Ashktorab,[1] M. D. Baker,[8] D. Beavis,[1] H. C. Britt,[7] J. Chang,[3] C. Chasman,[1] Z. Chen,[1] C.-Y. Chi,[4] Y. Y. Chu,[1] V. Cianciolo,[7] B. A. Cole,[4] H. J. Crawford,[2] J. B. Cumming,[1] R. Debbe,[1] W. Eldredge,[3] J. Engelage,[2] S. Y. Fung,[3] J. J. Gaardhoje,[12] M. Gonin,[1] S. Gushue,[1] H. Hamagaki,[5] A. G. Hansen,[12] L. Hansen,[12] G. Heintzelman,[8] S. Homma,[5] R. S. Hayano,[9] E. Judd,[2] J. H. Kang,[11] H. Kaneko,[6] A. Kumagai,[10] K. Kurita,[10] M. Levine,[1] J. Luke,[7] Y. Miake,[10] B. Moskowitz,[1] M. Moulson,[4] S. Nagamiya,[4] M. N. Namboodiri,[7] T. K. Nayak,[4] C. A. Ogilvie,[8] J. Olness,[1] L. P. Remsberg,[1] T. C. Sangster,[7] R. Seto,[3] K. Shigaki,[9] H. Sako,[5] R. Soltz,[7] S. G. Steadman,[8] G. S. F. Stephans,[8] T. Sung,[8] M. J. Tannenbaum,[1] J. H. Thomas,[7] S. R. Tonse,[7] S. Ueno-Hayashi,[10] F. Videbæk,[1] F. Q. Wang,[4] Y. Wang,[4] D. S. Woodruff,[8] Y. Wu,[4] G. Xu,[3] K. Yagi,[10] D. Zachary,[8] W. A. Zajc,[4] F. Zhu,[1] and Q. Zhu[3]

(E-802 Collaboration)

[1]*Brookhaven National Laboratory, Upton, New York 11973*
[2]*University of California, Space Sciences Laboratory, Berkeley, California 94720*
[3]*University of California, Riverside, California 92507*
[4]*Columbia University, New York, New York 10027*
and Nevis Laboratories, Irvington, New York 10533
[5]*Institute for Nuclear Study, University of Tokyo, Tokyo 188, Japan*
[6]*Kyoto University, Sakyo-Ku, Kyoto 606, Japan*
[7]*Lawrence Livermore National Laboratory, Livermore, California 94550*
[8]*Massachusetts Institute of Technology, Cambridge, Massachusetts 02139*
[9]*Department of Physics, University of Tokyo, Tokyo 113, Japan*
[10]*University of Tsukuba, Tsukuba, Ibaraki 305, Japan*
[11]*Yonsei University, Seoul 120-749, Korea*
[12]*Neil Bohr Institute, Copenhagen, Denmark*

(Received 26 August 1997)

Systematic results are presented on proton, deuteron, and triton emission from the target spectator region in collisions of 10.20*A* GeV gold projectiles with a gold target. A forward hodoscope utilizes detection of projectile spectator fragments to determine the orientation of the reaction plane, event by event. The directed flow $\langle p_x \rangle$ is determined as a function of pseudorapidity. Projectile spectator energy is used to estimate impact parameters. Results are compared to current theoretical models ARC, ART, and RQMD. In all cases good agreement with theory is obtained for calculations utilizing a pure cascade without nuclear potential contributions. [S0556-2813(98)00803-6]

PACS number(s): 13.85.Ni, 25.75.−q

I. INTRODUCTION

Over the past decade, the advent of relativistic heavy ion beams up to 14 GeV/*A* at BNL AGS and up to 200 GeV/*A* at CERN SPS have provided opportunities for the utilization of heavy ion collisions to begin studies of the properties of nuclear matter at new extremes of compression and energy density. Most recently the availability of very heavy beams of Au at AGS and Pb at SPS have allowed access to symmetric systems with total masses of the order of 400 nucleons [1]. Experiments at 1 GeV/*A* have shown experimental results sensitive to the nuclear equation of state [2,3]. The opportunity to explore this sensitivity in the 10 GeV/*A* regime is now available at the AGS. Central to all of these studies and their comparison to theoretical models are the degree to which the energy available in the collision is either thermalized among the collective degrees of freedom in the multiparticle system or conversely given directly to emitted nucleons or produced particles as a result of nucleon-nucleon collisions in the early stages of the intranuclear cascade. This paper presents results on particle emission in the target rapidity region for Au+Au collisions at 10.2*A* GeV. These results taken along with results at midrapidity in experiment E866 [4] and at projectile rapidity from experiment E877 [5] can begin to constrain the theoretical models and allow further insight into the basic reaction mechanisms.

At these high energies the simple spectator or participant model gives a good conceptual basis for discussing the broad characteristics of heavy ion reactions [6]. At finite impact parameters the nucleons in the participant region are involved in the first collisions with the subsequent direct emission of nucleons and produced particles. Some of the secondary particles escape and some are rescattered to begin the cascading that may ultimately lead to a thermalized (or partially thermalized) plasma of baryons and mesons. Under extreme conditions this plasma may transition to a quark-gluon plasma. On a longer time scale the thermalized participant region may then expand and the plasma may decay or hadronize into the baryons and mesons that are ultimately detected in the experiment.

In contrast to the complexity of interactions in the participant region, the physics of the spectator region is relatively simple. The spectator nucleons form a system that is excited by two distinct mechanisms and then is expected to decay statistically. First the rapid shearing process in the initial collision creates a nuclear system with many holes that when subsequently thermalized produce an internal excitation of a few MeV/A. At high energies this leads to a limiting fragmentation that has been predicted and observed in many cases [7]. The spectator region can be additionally excited by rescattering and absorption of particles from the participant region. Therefore, a detailed study of the subsequent decay of the spectator region may give sensitive tests to models of the cascade and energy damping in the participant region. For example, nucleon emission at angles behind the kinematic limits for nucleon-nucleon scattering is particularly sensitive to the internal Fermi momentum distribution of the participants and to rescattering in the participant or spectator.

The spectra of low energy nucleons emitted from the participant and spectator regions depend complexly on their excitation and any collective radial or directed flow that may be present. In the participant region the initial compression can lead to a radial collective expansion [8]. In general, at high bombarding energies it is expected that the spectator excitations will be modest and, additionally, there should be little compression of the spectator so that radial flow velocities will be small compared to the directed flow, ''bounce off'' component. This directed flow component results from the initial compression of the participant region and the ultimate bounce off of the spectator source. Preliminary observations of this bounce off component have been reported by both experiments E877 [9] and E866 [10] for Au+Au collisions at the AGS. Measurements of energy or momentum spectra for nucleons and complex fragments from the spectator region can, in principle, be used to sort out the effects of hydrodynamic flow from thermal excitation. The probability for emission of complex particles such as deuterons, tritons, and helium isotopes can also test coalescence models and, ultimately, may provide another measure of the excitation and degree of equilibration in the spectator.

Relativistic heavy ion collisions are so complex that it is generally impossible to gain significant physical insight into the underlying processes from the measurement and interpretation of a single observable. Instead there has been a close coupling between experiment and modeling to attempt a realistic portrayal of the complex kinematical conditions of the reactions. Then utilizing realistic transport models it may become possible to look for combinations of observables that will be sensitive to the underlying physical properties of the reactions, including thermalization, hadronization, and the thermochemical properties of the possible quark-gluon and baryon or meson plasma states that may be encountered at various stages of the reaction process.

At present several theoretical models are being developed which utilize the propagation of particles along classical trajectories with interactions adjusted to reproduce experimental scattering and reaction cross sections where known. The mix of particles in the cascade include the original nucleons as well as excited nucleon resonances and mesons created by the decay of nucleon resonances and strings. These models may or may not include a nuclear mean field. At AGS and higher energies the density of nucleon resonances and mesons in the initial collision becomes high enough that the cross sections for many unmeasureable processes such as nucleon and meson scattering, scattering involving nucleon resonances, and meson-meson scattering start to become important. Current models use a variety of reasonable assumptions for the forms of the unknown cross sections, the importance of the nuclear mean field and the mix of meson and baryons included. Several of these models have shown the ability to correlate, with a high degree of precision, inclusive observables and two particle correlations over a broad range of projectiles, ejectiles, and bombarding energy. However, the fact that models with quite different internal interaction properties and philosophies quantitatively fit much of the available data means that we need to move to the comparison of more exclusive correlations in order to provide meaningful tests of some of the more interesting underlying assumptions and parameters in the models. Models that reproduce a broad spectrum of inclusive data and have been applied to the prediction of collective flow phenomena at AGS energies include: ARC [11], ART 1.0 [12], and RQMD 1.07 [8,13].

In this paper we present spectra of low energy protons, deuterons, and tritons emitted at pseudorapidities, $-1.0<\eta<0.6$, and measurements of the directed flow $\langle p_x \rangle$, $\langle p_y \rangle$ in the same η interval. Results are presented as a function of impact parameter as determined from the energy deposited in a zero degree calorimeter. The experimental details and data analysis techniques are discussed in Sec. II, the inclusive spectra presented in Sec. III, the flow results presented in Sec. IV, and the data compared to model predictions in Sec. V. Section VI presents a summary and conclusions.

II. EXPERIMENTAL DETAILS

A. Experiment E866, general features

The results presented in this paper represent a subset of the data obtained in experiment E866 at the Brookhaven National Laboratory AGS facility. The data reported were obtained in the first full running period for E866 in the fall of 1993 using a 10.2A GeV gold beam on a gold target. A schematic layout of E866 is shown in Fig. 1. The experiment involves measurements in the midrapidity region using two spectrometers, Henry Higgins (HH) and the Forward Spectrometer (FS). Measurements in the target rapidity region were made with the highly segmented plastic scintillator phoswich array (PHOS). In addition the experiment provided impact parameter and reaction plane information on an event-by-event basis utilizing a zero degree calorimeter (ZCAL) which measured the number of spectator nucleons via their total energy and a small angle hodoscope (HODO) which measured the center of gravity of spectator protons relative to the beam center. Experiment E866 evolved from experiment E802 which studied Si reactions with HH and ZCAL and experiment E859 where the first version of the PHOS array was added. In experiment E866, the FS, HODO, and an expanded PHOS array were added. A detailed description of the E802 setup and the E859 PHOS array can be found in separate instrumentation papers [14,15].

The rapidity coverage of various detector systems in E866 is shown in Fig. 2 along with predictions of the mean proton

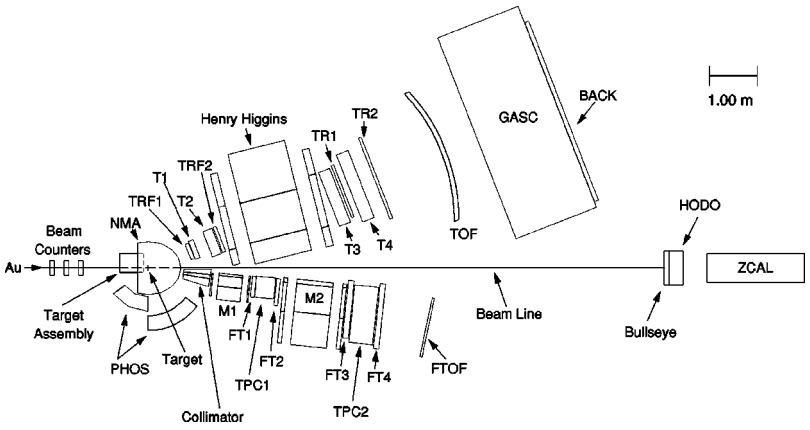

FIG. 1. E866 experimental layout.

transverse momentum in the reaction plane as a function of the proton rapidity using RQMD (version 1.07) [13,16]. The approximate rapidity ranges accessed by the various E866 detector subsystems are indicated.

Due to the symmetry of the Au+Au reaction, data complementary to the PHOS measurements could be obtained from the mean proton deflections in the HODO array but, in practice, the HODO acceptance and granularity is not sufficient to give a meaningful result. However, the E877 Collaboration does make a good measurement in this region using their forward spectrometer. Their results have already been reported [5] and are compared to the PHOS data in the discussion in Sec. V.

B. The PHOS array

The layout of the PHOS array is shown in Fig. 3. It consists of 100 ΔE-E phoswich [17] telescopes each read out using a single photomultiplier tube. Forty modules from the previous E859 array [15] were set up at angles between 90° and 140° at a distance of 65 cm from the target. A newly constructed array of 60 additional modules were positioned at forward angles between 40° and 90° at a distance of 100 cm. The forward 60 modules are shaped as truncated pyramids (solid angle of 1.9 msr) while the backward 40 modules are shaped such that each group of four forms a large truncated pyramid (each of the backward 40 modules subtends 3.8 msr). Both subarrays subtend approximately ± 10° in azimuth.

The fundamental operation and performance of each phoswich module is identical. The ΔE and time-of-flight information is provided by 5 mm of BC412, a fast scintillating plastic with short rise and decay times ($\tau_{\text{rise}}=1.0$ ns, $\tau_{\text{decay}}=3.3$ ns). The E section is 26 cm of BC444, a slower scintillating plastic with a relatively long rise time and a very long decay time ($\tau_{\text{rise}}=19.5$ ns, $\tau_{\text{decay}}=260$ ns). The signal from the photomultiplier tube (PMT) is split and integrated using two different ADC gates (60 and 220 ns in duration). This allows the signal components from the fast and slow scintillators to be unfolded. The ΔE-E and time-of-flight information are used to identify ''neutral'' particles, charged pions, protons, deuterons, and tritons over a broad range of kinetic energy (from 25 to 220 MeV for protons). The ''neutrals'' include γ's and neutrons which generally leave little or no energy in the thin fast plastic and charged particles which scatter into the module, missing the fast plastic. The response of the E859 phoswich modules to protons and deuterons of known incident energies was measured at the Indiana University Cyclotron Facility as described in [15]. This calibration forms the basis for the energy analysis of the p,d,t data shown below.

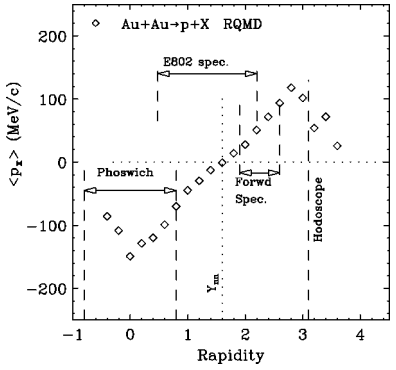

FIG. 2. Schematic illustration of the acceptance in rapidity of various E866 subsystems for the measurement of mean transverse momenta $\langle p_x \rangle$. The points represent predictions of the possible signal from an RQMD simulation for protons with no cuts on particle energy.

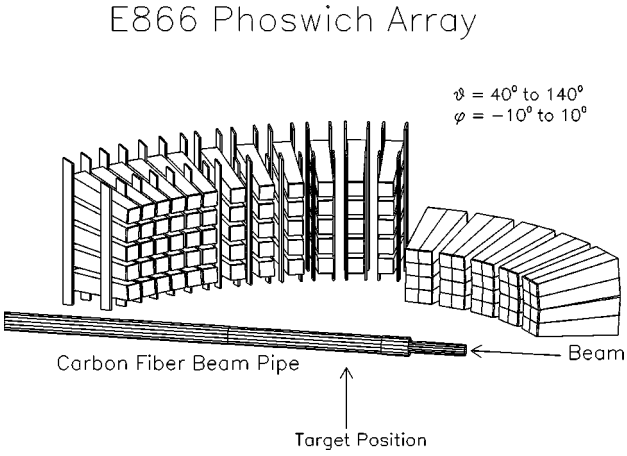

FIG. 3. Schematic layout of the phoswich scintillator (PHOS) subsystem in the E866 experiment.

TABLE I. Energy cuts used in flow analysis.

(a) Accepted kinetic energy ranges for identified particles

Particles	Energy range (MeV)
Protons	40–200
Deuterons	40–180
Tritons	45–145

(b) EZCAL cuts based on RQMD events

Imp. par (fm)	EZCAL range (GeV)
0–5	0–730
5–8	730–1280
8–10	1280–1580

(c) EZCAL cuts based on overlapping spheres

Imp. par (fm)	EZCAL range (GeV)
0–5	0–830
5–8	830–1420
8–10	1420–1740

Due to the simplified target geometry and thin carbon fiber target housing and beam pipe, the lower energy threshold for p,d,t detection in the PHOS array is mainly determined by the energy lost in the relatively thick (944 mg/cm^2) target. Unambiguous determination of the proton energy is possible for energies up to a maximum of 220 MeV. However, at the most forward angles, the high pion flux reduces the maximum proton energy for unambiguous identification (150 MeV) since multiple pion hits fall into the same region as the highest energy protons in ΔE-E space. This is a relatively small effect and there is little or no influence on the deuteron and triton measurements. The energy acceptance used to determine the mean p,d,t transverse momenta $\langle p_x \rangle$ and $\langle p_y \rangle$ are given in Table I.

C. The HODO array

HODO consists of two longitudinally coaxial scintillator slat arrays located directly in front of ZCAL. The two arrays are identical. Each array consisted of 39 identical slats of plastic scintillator (BC408) with dimensions of 1.0 cm$\times$0.8 cm$\times$40.0 cm. At either end, a curved Lucite light guide provided a mount for a 1/2-in. diameter phototube (a Hamamatsu R647 with 1.0-cm photocathode) so that the scintillator slats could be close packed. Indeed, care was taken to wrap the slats such that the total thickness of material was less than 3.0-mil per edge while maintaining light integrity (the total dead space between the slats was only slightly greater than 1% of the array area). Looking from the target, the first array was oriented for measurement in the horizontal X plane (vertical slats) and the following array (approximately 10 cm further downstream) for measurement in the vertical Y plane (horizontal slats). The distance from the target to the front of the X array was 10.5 m.

The signals from all 160 PMTs were processed into fastbus analog-to-digital converters (ADCs) and high resolution fastbus time-to-digital converters (TDCs). The signal from each PMT was split with a capacitive coupling to an ADC and a direct coupling to a fast discriminator which created the TDC input. The six center slats in each array had high current active bases to prevent gain changes due to the high particle flux and large pulse heights associated with beam particles. These slats also had a second lower gain output from an intermediate dynode stage to provide the dynamic range necessary to observe both beam (gold) particles and protons. The geometric mean of the two pulse heights from either end of a slat was calculated and normalized to give a constant output channel (250) for a single minimum ionizing hit (generally beam velocity protons). Typically, peaks corresponding to 1, 2, and 3 proton (or MIP) hits and a shoulder corresponding to $Z=2$ (essentially defined by Z^2 times the $Z=1$ peak location) are clearly visible in the pulse height spectra for individual slats. Timing cuts were generally applied to all slats after slewing corrections to eliminate particles that did not have the beam velocity. The timing resolution obtained using the R647 tubes with beam velocity particles was typically 250 ps.

For an individual event the mean charge centroid in each array was calculated. A number of weighting schemes were investigated for optimizing the sensitivity to the reaction plane. These included pulse height and the square root of the pulse height which are approximately proportional to charge squared and charge, respectively. Using the Monte Carlo simulation discussed below it was found that these two weighting schemes gave the best results and were approximately equivalent. In the final data reduction a weighting by pulse height was used.

Using the mean positions, the reaction plane for each event is determined by simply connecting the mean (X,Y) position of the spectator fragments on the HODO array with the estimated position of an undeflected beam particle. The determination of the beam location is complicated by the fact that the position of the beam at the HODO array sweeps during the beam spill. Indeed, the beam spot as well as the sweep length varied with the beam tune and consequently changed frequently during the measurements reported here. The sweep length was typically at least 1 cm in X and somewhat less in Y. This sweep adds a significant dispersion to the reaction plane determination. Fortunately, the beam spot and sweep were very predictable for a given tune. Therefore, a small sample of beam events was accepted into the trigger mix and used to determine the location of the beam spot on the HODO array as a function of time during the beam spill (typically about 600 ms). A functional form was fit to this dependence for each data run and used to estimate the beam position at the HODO array for each reaction event. In addition to the beam sweep there is a dispersion in the reaction plane determination due to the finite size of the beam profile at the HODO array which cannot be removed on an event-by-event basis. Using the beam event sample it was also possible to estimate the height or width of the beam on the X or Y HODO arrays and determine that this shape did not change significantly as a function of the spill time. The dispersion in the reaction plane determination due to the finite beam size is discussed in the next section.

D. Dispersion in reaction plane determination

A knowledge of the dispersion in the event-by-event reaction plane determination is essential for any comparison of azimuthal asymmetries to theoretical models. For example,

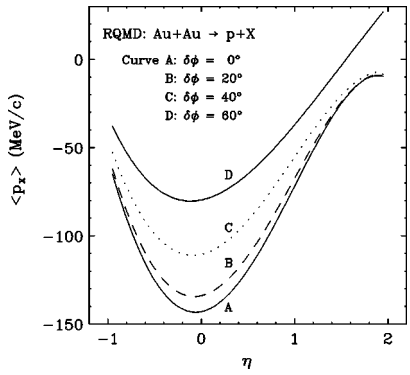

FIG. 4. Effect of a Gaussian dispersion with standard deviation $\delta\phi$ on the observed transverse momentum $\langle p_x \rangle$ distribution. The input distribution is taken from RQMD for protons with no cuts on particle energy.

Fig. 4 shows the effects of a Gaussian dispersion function with standard deviation $\delta\phi = 0°$, 20°, 40°, and 60° on the mean transverse momentum $\langle p_x \rangle$ calculated using the RQMD model.

There are several effects that can lead to a significant dispersion in the reaction plane measurement. From previous studies at the Bevalac [18] and SIS [19], it is known that the major component in the dispersion comes from the fluctuations due to the measurement of only a subset of the spectator particles. At best, this subset includes only the charged fragments but even within this set some are emitted at an angle too small to be very useful and a few at an angle too large to be detected. In previous measurements this effect tended to set a lower limit on $\delta\phi$ at about 30° [18,19]. In addition, in the present experiment there is significant dispersion due to the finite size of the beam spot. We believe that the dispersion due to the sweep of the beam spot across the HODO array during an AGS spill has been effectively removed by the technique described in the previous section. Other effects due to charge resolution, slat geometry and background hits in the HODO array have been studied and turn out to be significantly smaller than the inherent spectator fluctuation and beam spot size and when added in quadrature do not affect the final experimental dispersion.

A dispersion estimate that has been used previously at Bevalac [18] and also studied by the KAOS group [19] involves randomly subdividing every event into two subevents, each containing half the particles and then calculating a reaction plane for each subevent. The distribution of angles between the two subevents should have a width twice that expected for the full data sample. This technique does not include any instrumental effects such as the finite beam spot size. Additionally, there are possible correlation effects due to the use of independent slat arrays for X and Y as contrasted to the previous single array pad geometries. Nevertheless, we believe that this technique gives a useful lower limit for the dispersion. Results using this technique for our data are shown in Fig. 5 for all of the data and for three cuts in ZCAL which correspond to approximate impact parameter ranges of $b = 0$–5, 5–8, and 8–10 fm (see Table I). The results suggest a dispersion with $\delta\phi$ of approximately 37° independent of impact parameter. However, detailed Monte Carlo calculations described below give somewhat larger values especially for large and small impact parameters.

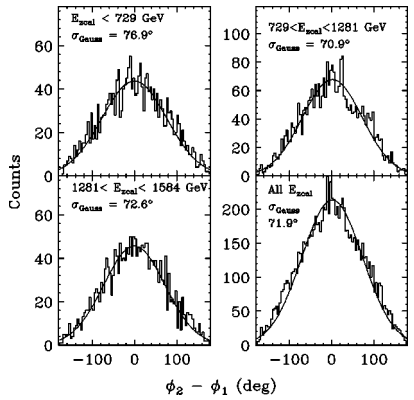

FIG. 5. The distribution of angles between two randomly selected subevents. Results are shown for cuts in EZCAL. The standard deviations for Gaussian fits to these distributions are shown in each case.

For a more detailed dispersion estimate, a full Monte Carlo of the experiment was developed using GEANT. This simulation included the target region, the beam pipe, the HODO array, and the ZCAL. An event generator was developed using RQMD events with $b = 0$–10 fm and a simple coalescence model to produce fragments [16]. The RQMD events used version 1.07 with the inclusion of nuclear potentials. The calculations gave a Z distribution approximating a power law with exponent -2.6. This value compares well to recently published emulsion data [20].

The distributions from the RQMD model for the difference between the estimated and the true reaction plane angles are shown in Fig. 6 and tabulated in Table II for a series of impact parameter ranges.

The results of these dispersion calculations are, in principle, sensitive to the p_T distributions in the event generator used (RQMD). In these calculations a set of events run with the inclusion of nuclear potentials was used but as shown later (Sec. V) these events do not give the best description of the directed flow observed in the data. In order to estimate the uncertainties in the estimated dispersion, due to the event

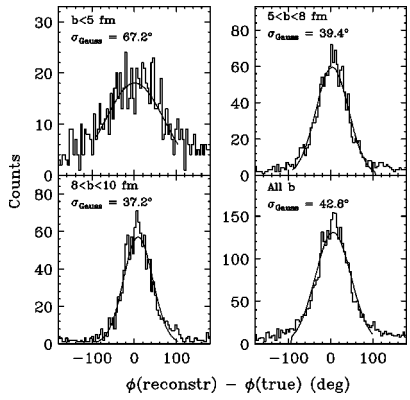

FIG. 6. Distributions in angle between the reconstructed reaction plane and the true reaction plane for protons taken from an RQMD event generator and transported in a GEANT simulation as described in the text. Results are presented for several regions of impact parameter. Distributions are fitted to Gaussian distributions over the region indicated by the solid lines. Fits yield the indicated standard deviations.

TABLE II. Standard deviations for a Gaussian fit to $\delta\phi$ distributions for dispersions with and without the effect of beam spot smearing (see text). In this table the column RQMD is for the event generator RQMD version 1.07 including nuclear potentials. The column $p_T\times 0.66$ modifies the events by multiplying transverse momenta of individual particles by 0.66. The column rect. beam adds the effect of a rectangular beam spot with dimensions 1.0 cm$\times$1.5 cm to RQMD. The column Gauss. beam adds the effect of a Gaussian beam spot with vertical or horizontal variances of 0.5 cm or 0.75 cm. The column Corr. factor gives, for each impact parameter bin, the correction factor to p_x corresponding to the $\delta\phi$ values in column 4, derived using RQMD events.

Impact parameter fm	$\delta\phi$ RQMD deg	$\delta\phi$ $p_T\times 0.66$ deg	$\delta\phi$ (rect. beam) deg	$\delta\phi$ (Gauss. beam) deg	Corr. factor
0–5	67	58	69	70	2.32
5–8	37	37	39	39	1.27
8–10	34	37	35	37	1.21
all	41	41	42	43	

generator, a separate calculation was run in which the p_T values for individual particles in each event were multiplied by 0.66. This corresponds to the maximal difference observed between all of the models with or without the inclusion of nuclear potentials. These results are included in Table II.

The results in Fig. 6 do not include the effect of the finite size beam profile at the HODO. In the experiment, the typical beam profile was rectangular with a width and height of approximately 1.0 and 1.5 cm, respectively. Simulations were performed assuming two extreme beam profile geometries, Gaussian with $\sigma=0.5$ and 0.75 cm for x and y directions, and a uniformly illuminated rectangle with (x,y) dimensions of 1.0 and 1.5 cm. Results of these calculations were added in quadrature to the intrinsic dispersions to give the estimated total dispersions in Table II.

We conclude that for $b=5$–10 fm, a dispersion function with $\delta\phi=35°-40°$ is most appropriate for this experiment. For $b<5$ fm or $b>10$ fm, the dispersions and their uncertainties become large and this technique becomes less reliable for determining quantitative azimuthal dependences.

E. Triggers and event sample

The data presented in this paper was taken as a part of the E866 run during the 1993 AGS cycle. The triggering scheme was similar to the earlier PHOS running in E859 [21]. A generic ''central trigger'' for E866 utilized ZCAL to isolate the 4% of events with minimum ZCAL to give the most central events. The generic E866 ''minimum bias'' trigger was generated by another cut on ZCAL at an energy just below the Au beam peak which allowed acceptance of all events in which the gold projectile loses at least one charge. The PHOS central and minimum bias triggers used in this analysis were then created by combining the generic E866 triggers with an additional requirement that at least one PHOS detector had an event. The ZCAL signal was also recorded event by event so that in the final analysis more restrictive windows could be placed on the number of participant nucleons.

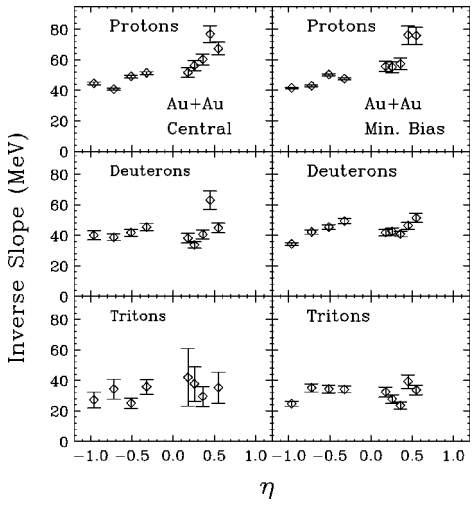

FIG. 7. Inverse slopes from the exponential fits to the experimental proton, deuteron, and triton spectra as a function of pseudorapidity.

The data presented were taken in dedicated PHOS runs and involved a total sample of approximately 60 000 events.

III. INCLUSIVE SPECTRA

Over the limited measurement region of the PHOS array the kinetic energy spectra obtained are reasonably represented by single exponentials $[d^3N/dp^3=C\ \exp(-E_{\rm kin}/B)]$. The inverse slopes obtained from these fits are shown in Fig. 7. The results show that in the target spectator region ($\eta<0$) the slopes are relatively independent of η and vary from about 45 MeV for protons to about 30 MeV for tritons. There is also little difference between central and minimum bias triggers.

Figure 8 shows distributions in $dN/d\eta$ summed over the energy region accepted by the PHOS array. Especially for $\eta>0$ it is known that the total spectra are not well described by a single exponential and since the PHOS measurements are limited to the lower energy part of the spectrum it is not possible to estimate the total rapidity or pseudorapidity distribution. A similar $dN/d\eta$ distribution was reported for the earlier Si + Au data [21] and for preliminary, low statistics Au+Au data obtained in 1992 with the E859 setup. A comparison of the current data with earlier Si+Au and p+Au for protons and deuterons is shown in Fig. 9. In the spectator region ($\eta<0$) the $dN/d\eta$ distributions are similar in shape. The magnitude of the low energy proton $dN/d\eta$ distribution is somewhat less for Au+Au than Si+Au. The difference in magnitude is even more pronounced for deuterons. This trend may reflect the larger and cooler spectators produced in the Si+Au relative to Au+Au systems.

Figure 10 shows the d/p and t/p ratios as a function of η for the limited energy acceptance of the PHOS array. Figure 11 shows d/p and t/p ratios as a function of ZCAL energy for the spectator region ($\eta<0$). The results indicate little dependence on η but a relative decrease in d and t for the most central collisions. These results are qualitatively consistent with a decrease in the relative production of complex particles in the most central collisions. In a simple coalescence picture this is consistent with a lower baryon density at freeze-out for the most central reactions.

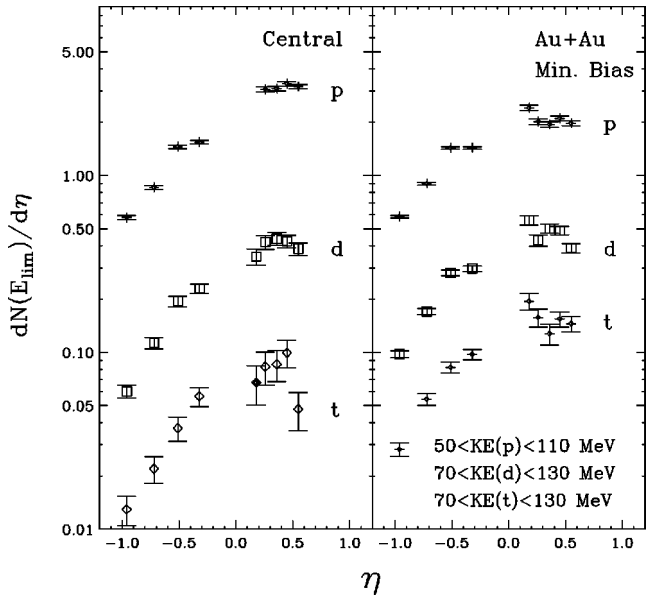

FIG. 8. Integrals of the kinetic energy spectra over the indicated energy ranges for protons, deuterons, and tritons as a function of pseudorapidity. Results are presented for Au+Au collisions with central and minimum bias triggers.

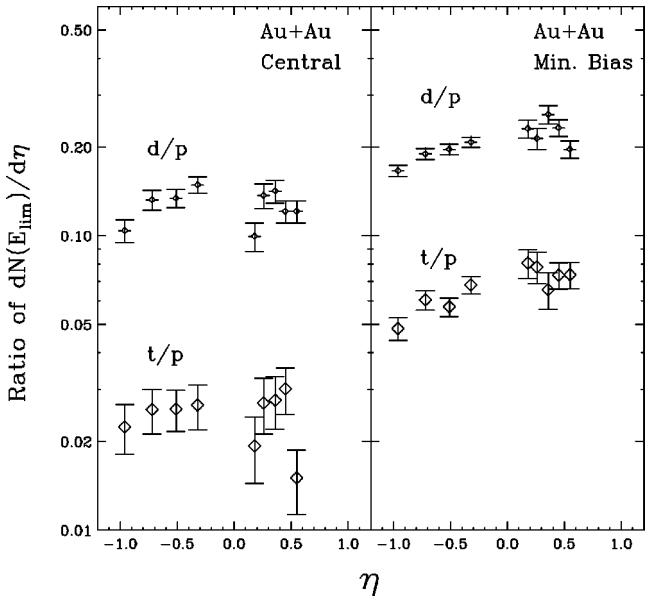

FIG. 10. Ratios of deuteron to proton and triton to proton emission rates as a function of pseudorapidity for central and minimum bias Au+Au collisions.

IV. DIRECTED FLOW

On an event-by-event basis, for each particle (p, d, or t) identified in a PHOS event, a total momentum is determined and projected on the reaction plane to yield a distribution of p_x and p_y in that plane. Figure 12 shows p_x spectra of p, d, t for a range $-0.12<\eta<0.05$. The results clearly show a shift to negative p_x which increases as the mass of the ejectile. This is a clear sign for a directed flow component.

Figure 13 shows a composite of results for p_x and p_y for p, d, and t. On the top are contour plots of p_x vs p_y which show a shift to negative p_x increasing with ejectile mass. The results also show symmetry in p_y. In this plot a ''squeeze-out'' component would show up as a bulge at $\pm\, p_y$. Within the statistical accuracy of this data, such a component is not observed in this rapidity region. However, in experiment E877, a slightly elliptical flow was observed in the reaction plane [9]. Mean p_x and p_y values are shown as a function of EZCAL and η in the lower panels. The results show mean p_y consistent with 0 everywhere which provides a test of the accuracy of the mean beam position determination. The range 730 GeV$<$EZCAL$<$1580 GeV corresponds, approximately, to the $b=5$–10 fm region where the reaction plane determination is most reliable. Below EZCAL=730 GeV and above EZCAL=1580 GeV, the dispersion corrections begin to increase significantly and may account in part for the apparent decrease in the absolute value of the mean p_x, ($|\langle p_x\rangle|$). As a function of η the results show a maximum in $|\langle p_x\rangle|$ near $\eta=0$ as predicted in most calculations.

Figure 14 shows values of $\langle p_x\rangle/A$ versus η for four bins

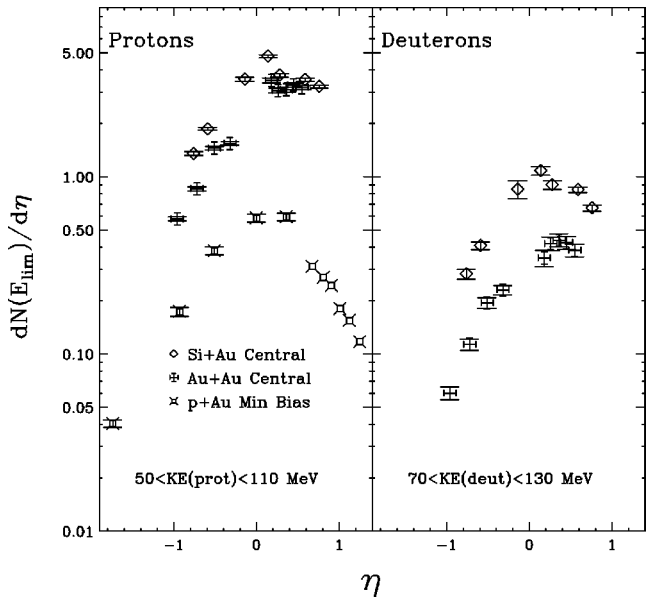

FIG. 9. Integrals of the kinetic energy spectra over the indicated energy ranges for protons and deuterons as a function of pseudorapidity. Results are presented for central triggers for Si+Au, Au +Au, and min bias p+Au collisions.

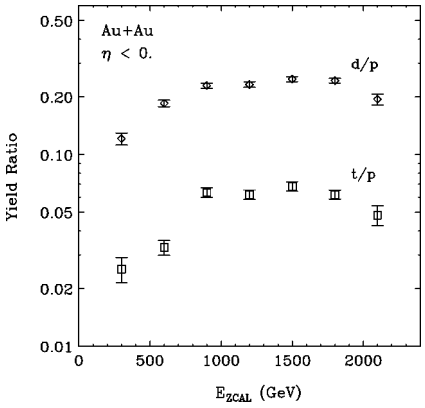

FIG. 11. Ratios of deuteron to proton and triton to proton emission rates for pseudorapidity less than zero as a function of energy in the zero degree calorimeter (ZCAL).

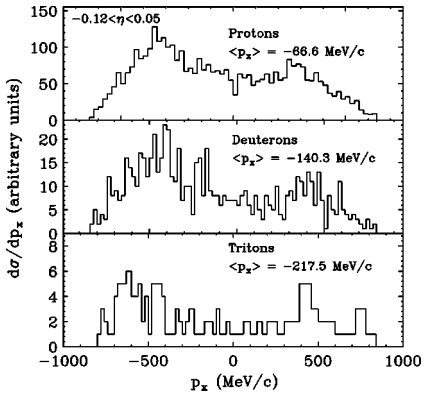

FIG. 12. Typical transverse momentum distributions for protons, deuterons, and tritons in the indicated pseudorapidity range.

of EZCAL which correspond qualitatively to $b=0$–5, 5–8, 8–10, and 10–14 fm ranges in impact parameter. The ZCAL correlation to impact parameter is obtained by estimating the total energy in spectators from RQMD at impact parameters of 5, 8, and 10 fm to be 730, 1280, and 1580 GeV, respectively. A purely geometric correlation to EZCAL would give somewhat higher values for the cuts (830, 1420, and 1740 GeV) but within the statistical uncertainties of the data would not change any of the conclusions in the next section.

For the center two bins and for minimum bias data where the corrections are minimum, the $\langle p_x\rangle/A$ values for protons have been corrected for dispersion ($\delta\phi$) using values listed in Table II (column ''$\delta\phi$ / rect. beam''). The correction factors for each impact parameter and η bin was obtained from RQMD simulations by comparing the $\langle p_x\rangle/A$ values with and without ϕ dispersion. The average correction factor for each impact parameter bin is given in Table II. The uncorrected and corrected distributions for a minimum bias trigger for protons are shown in Fig. 15 to indicate the general magnitude of the dispersion correction. The estimated systematic uncertainty in the values determined for $\delta\phi$ is $\pm 3°$ which would lead to an additional systematic uncertainty of approximately ± 5 MeV/c for the maximum $|\langle p_x\rangle|$ values shown in Fig. 15 and in the following section. The dispersion corrected distributions are compared to various models in the next section.

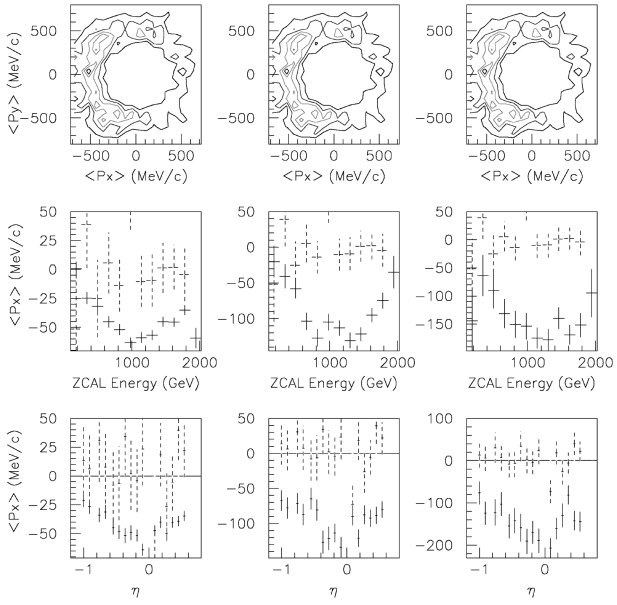

FIG. 13. Mean transverse momentum $\langle p_x\rangle$ as a function of $\langle p_y\rangle$, ZCAL energy, and pseudorapidity for protons (left), deuterons (center), and tritons (right). Points with dashed error bars are for $\langle p_y\rangle$. The transverse momenta have not been corrected for dispersion in the reaction plane determination.

Qualitatively, the results show that the maximum $|\langle p_x/A\rangle|$ values are independent of particle type.

V. MODEL COMPARISON

Most current results suggest that the AGS energy regime (10–15 A GeV) is close to optimum for studies of the maximum baryon densities achievable in relativistic heavy ion collisions. Studies of collective flow phenomena may be an important tool for determining the compression achieved, the importance of compression and heating on microscopic scattering processes, and the magnitude of the damping of energy from initial kinetic modes to thermal and collective modes. Currently there are three theoretical models which have been able to quantitatively characterize hadron and produced particle inclusive distributions for AGS Au+Au experiments and have gone on to make predictions on flow quantities. These models (ARC [11], ART 1.0 [12], and RQMD 1.07 [13]) are all microscopic relativistic collision models including baryons, produced mesons, and resonances. They all use experimental interaction cross sections where available. They, however, differ significantly in how they handle the particle transport during the collision process. All models also find that at these energies the dynamics of the rescattering of resonances are important and here little or no measured cross section data is available. A current question of interest and debate is the relative importance of including nuclear mean field effects in an intranuclear cascade model at these energies. It is expected that the collective flow may be an important observable for evaluating the importance of mean field effects.

The ARC model [11] is a pure cascade which has been successful in correlating a large volume of data from Bevalac to AGS energies. This model is able to reproduce quite well flow from the EOS data at Bevalac and the E877 experiment at AGS [22]. This agreement requires a restriction to repulsive scattering at low collision energy ($E_{\rm col}<300$ MeV) and phasing into diffractive scattering, equal repulsive and attractive scattering, at higher energies ($E_{\rm col}>500$ MeV). Using various coalescence techniques this model has also been used to predict distributions for complex particles such as deuterons [23].

ART 1.0 [12] is based on the BUU transport model used for intermediate energy heavy ion collisions by including more baryon and meson resonances as well as interactions between them. The set of resonances included is not as extensive as in some other models but the authors believe that ''the effects of heavier baryon resonances are partially included by using meson+baryon cross sections calculated from the implicit formation of these heavier resonances with masses up to 2 GeV.'' This model has the option of including nuclear mean field effects in the baryon scattering.

RQMD 1.07 [13] is a semiclassical transport model using

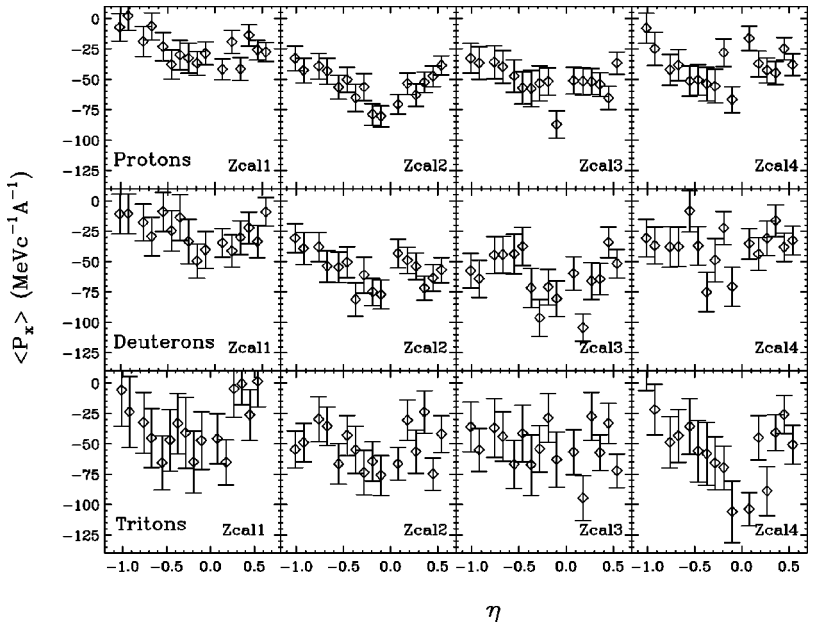

FIG. 14. Mean transverse momentum $\langle p_x \rangle$ as a function of pseudorapidity for four ranges of ZCAL energy for protons, deuterons, and tritons. The ranges used are ZCAL1=0–730 GeV, ZCAL2=730–1280 GeV, ZCAL3=1280–1580 GeV, ZCAL4>1580 GeV. These results have not been corrected for dispersion in the reaction plane determination.

the relativistic quantum molecular dynamic approach. This combines the classical propagation of particles with the excitation of hadrons into resonances and strings. Secondaries subsequently undergo interaction with each other and with ingoing baryons. Since real particles are transported there is the option of calculating cluster formation at freeze-out. This model includes the option of a density dependent quasipotential between baryons. This model has been successful in reproducing AGS inclusive data. In this section we will show some detailed comparisons of proton distributions to RQMD (version 1.07) calculations done in Livermore during 1993–1994 [16].

To compare the experimental results with the theoretical calculations it is essential to take into account both the dispersion and the limited acceptance present in the experimental data. In Sec. II D the estimated effects due to the angular dispersion in the determination of the reaction plane have been discussed. The other major acceptance effect is due to the finite energy acceptance for the measurements. The energy acceptance ranges for p, d, and t in the experimental data used in the $\langle p_x \rangle$ determinations are shown in Table I. In the spectator region ($\eta<0$) the major acceptance effect is due to a low energy cutoff in the PHOS detectors. In this region virtually all of the particles above these cutoffs are included in the measured spectra. However, for $\eta>0$ the spectra begin to include more high energy particles from the participant region and the exclusion of the high energy tail from the measurements has a significant effect. Since the effects of these unmeasured tails depends on the shape of the spectra in unmeasured regions, it is not possible to correct the data for the energy cutoffs in a model independent manner.

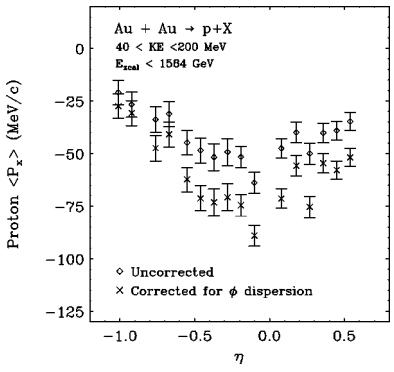

FIG. 15. Mean transverse momentum $\langle p_x \rangle$ for protons with minimum bias trigger. Measured values and values corrected for dispersion in the reaction plane determination are presented.

Figure 16 (using RQMD 1.07 with potentials) shows that the exclusion of high and low energy portions of the proton spectra can have a very large effect on the $\langle p_x \rangle$ distribution. Introducing a 40 MeV low energy cutoff increases the apparent $|\langle p_x \rangle|$ value especially in the spectator region. As expected the high energy cutoff has only a small effect in the spectator region but decreases the values of $|\langle p_x \rangle|$ in the participant region, $\eta>0$. Because of this sensitivity it is important to compare experiment and theory for both inclusive and $\langle p_x \rangle$ distributions and to use the experimental energy cuts in the theoretical predictions.

The RQMD calculations used in this paper contain events in the impact parameter range $b=0$–10 fm [16]. These RQMD calculations contain both events run in cascade mode (a total of 2000 events) and events which include nuclear potentials (a total of 3700 events). The experimental minimum bias trigger is approximately equivalent to the range $b=0$–14 fm. Thus, to make a direct comparison it is necessary to define a new trigger condition (b_{RQMD}) which effectively limits the data to the range $b=0$–10 fm. This condition was used for the data sort by requiring EZCAL<1580 GeV.

Figure 17 shows absolute comparisons of the RQMD (version 1.07 with potentials) predictions with measured proton

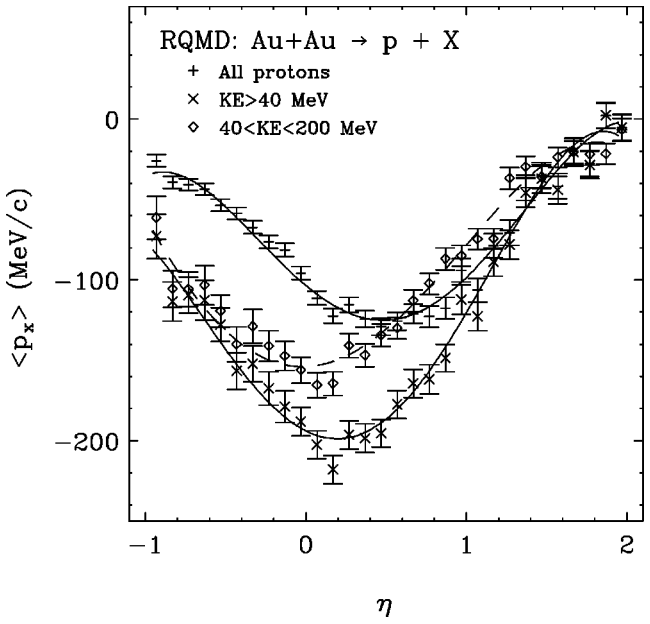

FIG. 16. Mean transverse momentum $\langle p_x \rangle$ for protons as a function of pseudorapidity from an RQMD event generator with various cuts in the proton energy acceptance.

energy spectra at four angles. In this comparison the b_{RQMD} trigger condition discussed above is used for the data sort and the RQMD calculation is for $b=0$–10 fm. It is seen that overall the absolute agreement between data and prediction is reasonable with a significant overprediction only at the most forward angle (60°). The RQMD spectra show a somewhat smaller slope parameter resulting in an overprediction of the data at the lowest energies. This overprediction at low energies may just reflect the limited accuracy of the mass surface and complex fragment production in this version of RQMD which was not designed to look in detail at coalescence in the spectator region. It is more remarkable that RQMD does such a good job of absolutely predicting the angular and energy dependence of the data.

Figure 18 shows a comparison of the dispersion corrected data for the b_{RQMD} trigger compared to RQMD (version 1.07) calculations with and without the inclusion of nuclear potentials. Within statistics the data and the pure cascade calculation agree. Our limited RQMD event set restricts the statistical accuracy of the model calculations and precludes more exclusive comparisons as a function of impact parameter (ZCAL). The interpretation of our apparent agreement with the cascade calculation is unclear at the moment. Similar flow measurements from experiment E877 in the projectile spectator region have been compared to RQMD (version 2.3) [5] and in this case the results agree best with the calculations which include nuclear potentials. As discussed below our data and the E877 data appear to be in agreement when their relative acceptances are taken into account. The major difference between RQMD versions 1.07 and 2.3 is a change in the scattering cross sections which results in decreased flow from the cascade calculation for version 2.3. This decrease in flow can be made up by including nuclear potentials. These comparisons suggest that the underlying uncertainties in the models are of the same magnitude as the inclusion or exclusion of nuclear potential effects.

Figure 19 shows a comparison of dispersion corrected data for impact parameter ranges $b=5$–8 fm (EZCAL $=730$–1280 GeV), $b=8$–10 fm (EZCAL$=1280$–1580 GeV), and $b=0$–14 fm (min bias) to calculations using the ART model. The dispersion corrections have been done using values given in Table II. The results show that the data track the cascade calculation in all cases. The addition of a soft equation of state modifies the minimum $\langle p_x \rangle$ in an impact parameter sensitive manner which does not appear to be represented in the data set. However, the addition of approximately 5 MeV/c systematic uncertainties in the dispersion

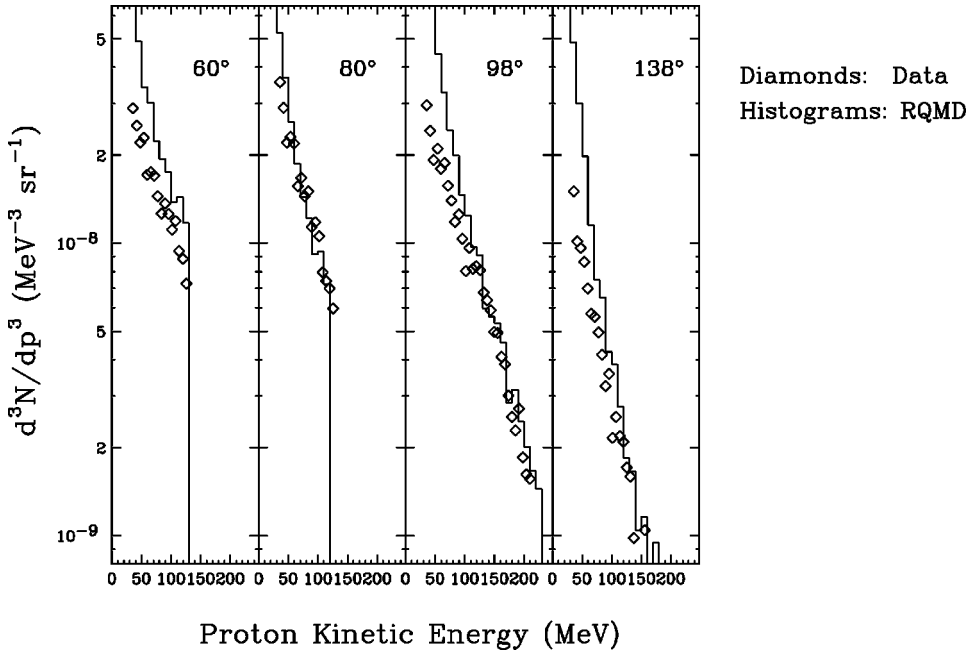

FIG. 17. Absolute comparison of proton energy spectra from data and RQMD simulation. Points are experimental data and histogram is RQMD prediction. Calculations and data are for the impact parameter range $0<b<10$ fm.

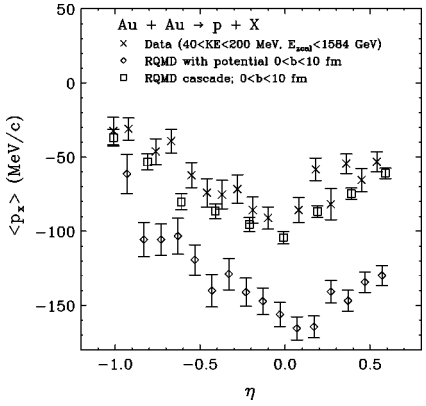

FIG. 18. Comparison of mean transverse momenta $\langle p_x \rangle$ for protons with b_{RQMD} trigger (see text) with predictions from RQMD in cascade mode and with inclusion of nuclear potentials. Calculations and data are for the impact parameter range $0<b<10$ fm. The experimental data have been corrected for the effects of dispersion in the reaction plane determination as discussed in the text.

corrections and the relatively small difference in the flow as a result of including nuclear potentials do not allow a definitive exclusion of the calculations with potentials.

In Ref. [24], a comparison has been made between the uncorrected proton data shown in Fig. 14 and results of calculations using the ARC code and a Monte Carlo filter that reproduces the HODO and PHOS acceptances. Here it is again seen that the results are in good agreement with calculations from a cascade model without inclusion of nuclear potential effects. However, this cascade does have a restriction to repulsive scattering at low energies which is not included explicitly in the other models.

A measurement [5,9] in the region of the projectile spectator in AGS experiment E877 shows a maximum, dispersion corrected $|\langle p_x \rangle|$ of 100–120 MeV/c for protons at rapidities slightly less than beam rapidity. This result can be compared to the value of 80–100 MeV/c shown in Fig. 15 for target rapidity ($\eta=0$). However, as Fig. 16 shows the exact values

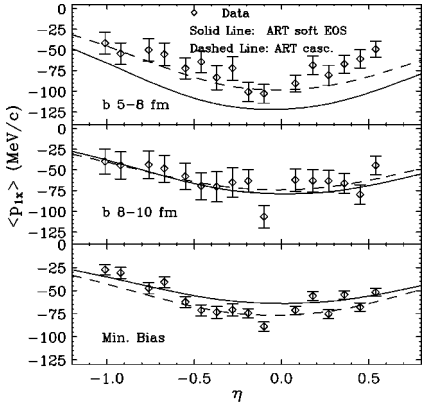

FIG. 19. Comparison of mean transverse momenta $\langle p_x \rangle$ for protons with minimum bias triggers with predictions from ART in cascade mode and with inclusion of nuclear potentials. Calculations for impact parameter ranges $b=5$–8 and 8–10 fm are compared to data gated on appropriate ranges in ZCAL energy as described in the text. The experimental data have been corrected for the effects of dispersion in the reaction plane determination as discussed in the text.

of $\langle p_x \rangle$ at a given η or rapidity (Y) are quite sensitive to the acceptance in energy or momentum for the experiment. Therefore, a simple comparison of $|\langle p_x \rangle|$ may not be a reliable measure of the consistency of data from the two experiments. A better comparison has been made where both the data presented here and the detailed flow tensors measured in experiment E877 were compared in detail to ARC calculations [24]. In both cases remarkably good agreement is found between data and predictions for ARC using realistic experimental acceptance filters. We conclude that within the stated statistical and systematic errors the two measurements are in agreement.

The comparisons discussed above indicate that all three models ARC, ART, and RQMD are capable of reproducing a dynamical variable such as flow at AGS energies. It is important to note that in all cases the flow calculations from all three models are predictive with no adjustment of parameters beyond those cross sections determined previously in comparisons to participant inclusive data. In the 1994 E866 data there is a much more detailed data set involving azimuthal correlations for p,d,t, He, and produced particles which may give even more stringent tests to current theoretical models.

VI. SUMMARY AND CONCLUSIONS

The results presented in this paper show spectra and directed flow $\langle p_x \rangle$ for protons, deuterons, and tritons from the target spectator region in Au+Au collisions at AGS. The results are consistent with a modestly excited spectator fragment and show a relative decrease in complex particle emission (d/p and t/p) in the most central collisions. This general feature is expected from most general models and predicted in current versions of ARC [24] and RQMD [8,16]. Theoretical calculations using ARC, ART, and RQMD all predict the measured flow when restricted to a pure cascade calculation. The predictions deviate from the data when nuclear potentials are included in ART and RQMD. However, a more recent version of RQMD, version 2.3, appears to require the inclusion of nuclear potentials in order to fit similar E877 flow results [5]. Most remarkable is that these models which have been developed to reproduce and are compared to high energy participant data continue to work in a quantitative manner when compared to detailed data from the spectator region. Future experiments with better statistical accuracy may allow more exclusive comparisons to further investigate the role of nuclear potentials in these collisions.

ACKNOWLEDGMENTS

We are pleased to acknowledge the many contributions from and useful discussions with Georg Peilert during the early phases of this project. We are grateful to D. E. Kahana, R. Mattiello, B. A. Li, and C. M. Ko for making available predictions from their theoretical models for comparison with the experimental data. In addition one of us (H.C.B.) is pleased to acknowledge support from the Alexander von Humboldt Stiftung, very useful discussions with H. H. Stöcker, W. Greiner, and the hospitality of the Theoretical Nuclear Physics Institute, University of Frankfurt during part of the development of this manuscript. We are grateful to the

accelerator operations staff at the BNL Tandem and AGS accelerators and to the staff of the BNL AGS department for their contributions to the development of the E866 experiment and its successful operation. This work is supported by the U.S. Department of Energy under contracts with BNL (Grant No. DE-AC02-76CH00016), Columbia University (Grant No. DE-AC02-76ER03069), LLNL (Grant No. W-7405-ENG-48), MIT (Grant No. DE-AC02-76ER03069), UC Riverside (Grant No. DE-FG03-86ER40271), by NASA under contract with the University of California (Grant No. NGR-05-003-513), by the Ministry of Education (Grant No. BSRI-96-2426), and KOSEF (Grant No. 951-2020-032-2) in Korea, and by the Ministry of Education, Science and Culture of Japan under the Japan-U.S. agreement on cooperation in High Energy Physics.

[1] *Proceedings of Quark Matter '91* [Nucl. Phys. **A544** (1992)]; *Quark Matter '93* [*ibid.* **A566** (1994)]; *Quark Matter '95* [*ibid.* **A590** (1995)].

[2] H. H. Gutbrod, A. M. Pozkanzer, and H. G. Ritter, Rep. Prog. Phys. **52**, 1267 (1989), and references therein.

[3] H. Stöker *et al.*, Phys. Rev. C **25**, 1873 (1982); H. Stöcker and W. Greiner, Phys. Rep. **137**, 277 (1986), and references therein.

[4] Y. Akiba for the E866 Collaboration, in *Proceedings of Quark Matter '96* [Nucl. Phys. **A610**, 139c (1996)].

[5] T. K. Hemmick for the E877 Collaboration, in *Proceedings of Quark Matter '96* [Nucl. Phys. **A610**, 63c (1996)]; in Proceedings of the Winter Workshop on Nuclear Dynamics, Marathon, Florida, 1997 (unpublished).

[6] J. D. Bowman, W. J. Swiatecki, and C. F. Tsang, Lawrence Berkeley Laboratory Report No. LBL-2908, 1973 (unpublished); J. Hüfner, K. Schäfer, and B. Schürmann, Phys. Rev. C **12**, 1888 (1975).

[7] A. S. Goldhaber, Phys. Lett. **53B**, 306 (1973).

[8] R. Mattiello, H. Sorge, H. Stöcker, and W. Greiner, Phys. Rev. C **55**, 1443 (1997).

[9] J. Barrette *et al.*, Phys. Rev. Lett. **70**, 2996 (1993): **73**, 2532 (1994); Nucl. Phys. **A590**, 557c (1995).

[10] H. C. Britt, M. N. Namboodiri, and T. C. Sangster, in Proccedings of International Conference on Nuclear Physics at the Turn of the Millennium: Structure of the Vacuum and Elementary Matter, Wilderness, South Africa, 1996, edited by H. Stöcker (World Scientific, Singapore, 1996), p. 538.

[11] Y. Pang, T. J. Schlagel, and S. H. Kahana, Nucl. Phys. **A544**, 435c (1992); S. H. Kahana, T. J. Schlagel, and Y. Pang, *ibid.* **A566**, 465c (1993); Y. Pang, D. E. Kahana, S. H. Kahana, and T. J. Schlagel, *ibid.* **A590**, 565c (1995).

[12] B. A. Li and C. M. Ko, Phys. Rev. C **52**, 2037 (1995); report, 1996 (unpublished).

[13] H. Sorge, H. Stöcker, and W. Greiner, Ann. Phys. (N.Y.) **192**, 266 (1989); Nucl. Phys. **A498**, 567c (1989).

[14] T. Abbott *et al.*, Nucl. Instrum. Methods Phys. Res. A **290**, 41 (1990).

[15] J. B. Costales, H. C. Britt, M. N. Namboodiri, T. C. Sangster, J. H. Thomas, and H. E. Wegner, Nucl. Instrum. Methods Phys. Res. A **330**, 183 (1993).

[16] G. Peilert (private communication).

[17] D. H. Wilkinson, Rev. Sci. Instrum. **23**, 414 (1952); For a more recent application see A. Baden *et al.*, Nucl. Instrum. Methods Phys. Res. A **203**, 189 (1982).

[18] P. Danielewicz and G. Odyniec, Phys. Lett. **157B**, 147 (1985).

[19] D. Brill *et al.*, Z. Phys. A **355**, 61 (1996).

[20] G. Singh and P. L. Jain, Phys. Rev. C **49**, 3320 (1994); P. L. Jain, G. Singh, and A. Mukhopadhyay, Phys. Rev. Lett. **74**, 1534 (1995).

[21] L. Ahle *et al.*, Phys. Rev. C **55**, 2604 (1997).

[22] D. E. Kahana, D. Keane, Y. Pang, T. Schlagel, and S. Wang, Phys. Rev. Lett. **74**, 4404 (1995); D. E. Kahana, Y. Pang, and E. Shuryak, Phys. Rev. C **55**, 481 (1997).

[23] D. E. Kahana, S. H. Kahana, Y. Pang, A. J. Balz, C. B. Dover, E. Schnedermann, and T. J. Schlagel, Phys. Rev. C **54**, 338 (1996).

[24] D. E. Kahana, in *Proceedings of the HIPAGS '96 Conference*, Detroit, Michigan, edited by C. A. Pruneau *et al.* (Wayne State University, Detroit, 1996), p. 126.